JACS Au
AN OPEN ACCESS JOURNAL OF THE AMERICAN CHEMICAL SOCIETY

pubs.acs.org/jacsau

Article

Defect-Induced Magnetic Skyrmion in a Two-Dimensional Chromium Triiodide Monolayer

Ryan A. Beck, Lixin Lu, Peter V. Sushko, Xiaodong Xu, and Xiaosong Li*

Cite This: *JACS Au* 2021, 1, 1362–1367

Read Online

ACCESS | Metrics & More | Article Recommendations

ABSTRACT: Chromium iodide monolayers, which have different magnetic properties in comparison to the bulk chromium iodide, have been shown to form skyrmionic states in applied electromagnetic fields or in Janus-layer devices. In this work, we demonstrate that spin-canted solutions can be induced into monolayer chromium iodide by select substitution of iodide atoms with isovalent impurities. Several concentrations and spatial configurations of halide substitutional defects are selected to probe the coupling between the local defect-induced geometric distortions and orientation of chromium magnetic moments. This work provides atomic-level insight into how atomically precise chemical doping can be used to create and control complex magnetic patterns in chromium iodide layers and lays out the foundation for investigating the field- and geometric-dependent magnetic properties in similar two-dimensional materials.

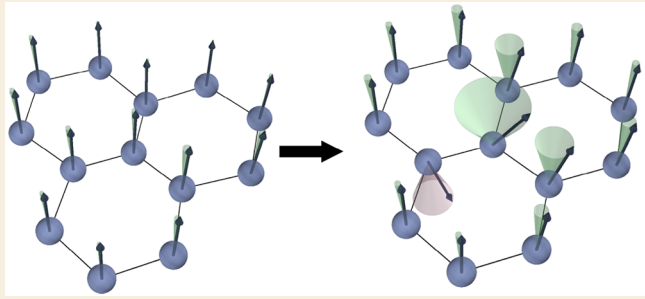

KEYWORDS: *2-D magnetism, chromium triiodide, Density Functional Theory, skyrmion, thin film, anion replacement*

INTRODUCTION

Magnetic skyrmions are local whirls of the spins that both have a fixed chirality and do a full spin rotation.[1,2] Isolated skyrmions can be treated as single particles and used in applications, such as system memory and radio-frequency generators and filters, as well as spintronic devices.[1,3−5] Magnetic skyrmions have been found to be manifested in both single crystals of magnetic materials such as MnSi, FeGe, $Fe_{1-x}Co_xSi$, and Cu_2OSeO_3 as well as in thin films such as Fe monolayers and PdFe bilayers on Ir.[1,4] In order for a skyrmion to be usable for memory or spintronic applications, however, they need to be realizable at, or close to, room temperature and with minimal electromagnetic fields.

Skyrmions form in crystals when they lack inversion symmetry in the crystal lattice, enabling the formation of Dzyaloshinskii−Moriya interactions (DMIs) through spin−orbit coupling, or in the case of thin films at the interface between the layer and the substrate facilitated through the strong spin-orbit coupling of the nearby metal center.[1,4] This DMI takes the form[6]

$$H_{\mathrm{DMI}} = (S_1 \times S_2)\cdot \mathbf{D}_{12} \quad (1)$$

where S_1 and S_2 are spins of two neighboring magnetic atoms and $\mathbf{D}_{12}$ is the corresponding Dzyaloshinskii−Moriya vector. If the exchange interaction between S_1 and S_2 is mediated by an anion, $\mathbf{D}_{12}$ can be approximated as $\mathbf{D}_{12} = \mathbf{r}_1 \times \mathbf{r}_2$, where $\mathbf{r}_1$ and $\mathbf{r}_2$ link the anion with the two magnetic ions.[7] In materials containing inversion symmetry, this term is missing, as the contributions associated with anionic pathways linking magnetic centers cancel out.

Chromium trihalides and, more broadly, MX_3 (where M is a transition metal) compounds have been actively investigated for their unusual properties. They have a low synthesis and processing cost and can be easily exfoliated to obtain few-layer materials. In chromium trihalide (CrX_3, X = Cl, Br, I) structures, the Cr^{3+} ions are arranged into honeycomb lattices surrounded by six halogen anions, giving rise to a local octahedral symmetry. The halogen atoms are each bound to two neighboring Cr centers. At high temperature the layers stack with a monoclinic (space group $C2/m$) geometry. At low temperature the layers stack with a rhombohedral (space group $R\bar{3}$) geometry. The temperature at which this transformation occurs is dependent on the halogen (Cl, 240 K; Br, 420 K; I, 210 K), and each bulk structure is known to have ferromagnetic moments between each Cr ion below their T_c values (Cl, 17 K; Br, 37 K; I, 68 K).[8,9] Examples of the monolayer, hexagonal lattice can be seen in the insets to Figure 1.

Received: March 29, 2021
Revised: June 30, 2021
Accepted: July 1, 2021
Published: July 13, 2021

ACS Publications

© 2021 The Authors. Published by American Chemical Society

https://doi.org/10.1021/jacsau.1c00142
JACS Au 2021, 1, 1362–1367

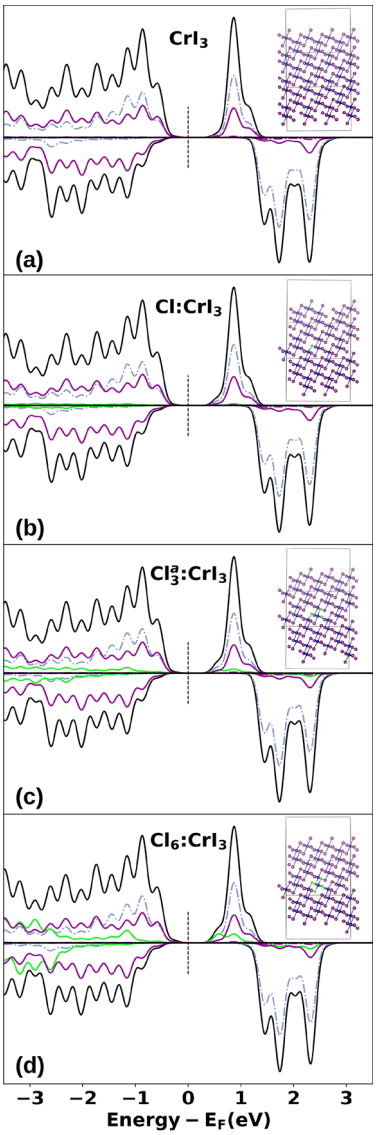

Figure 1. Spin-resolved projected density of states for the monolayer CrI_3 systems (shown as insets to each plot). The total DOS can be seen in each plot as the black line, and the projected orbital contributions for the Cr d (blue) and I p (purple), and Cl p (green) atoms are plotted as well. The pure CrI_3 monolayer is shown at the top (a), with the halogen-replaced structures shown beneath: $Cl:CrI_3$ (b); $Cl_3^a:CrI_3$ (c); $Cl_6:CrI_3$ (d).

It has been shown that in the low-layer limit (number of layers $\lesssim$10), MX_3 exhibits magnetic properties that appear to differ from their bulk properties.[10−13] Recently, mono- and bilayers of chromium trihalide materials have been investigated for potential use in skyrmionic devices.[1,3,14,15] Of the chromium trihalides, chromium triiodide (CrI_3) materials have been of the most interest, as bulk CrI_3 has been shown to exhibit the highest reported magnetic ordering temperature and anisotropy among the chromium trihalides.[8,10,16−18]

Monolayer CrI_3, in disagreement with the Mermin−Wagner theorem, is known to have long-range ferromagnetic character[3,19] that is enabled through the magnetic anisotropy.[3,20] This magnetic anisotropy in CrI_3 arises from the spin−orbit coupling in iodine atoms and favors a magnetic easy axis perpendicular to the atomic plane.[7,9,20] Magnetic interactions between the chromium ions in a CrI_3 layer arise from a superexchange mechanism between the Cr 3d orbitals and the I 5p orbitals.[7,13,20,21] Geometric distortions in the CrI_3 layers can break the inversion symmetry and thus induce finite Dzyaloshinskii−Moriya interactions, ultimately leading to the appearance of skyrmionic ground states. In the case of an applied electric field oriented perpendicular to the CrI_3 plane, the Cr^{3+} and I^- ions are displaced in opposite directions out of their atomic planes. These displacements change distances between the chromium and iodine atomic planes by as much as ∼3.6% for a field with a magnitude of ∼0.2 V/nm, which breaks the inversion symmetry and results in significant DMI effects. It has also been reported that Janus $Cr(I,X)_3$ monolayers have been able to realize ground-state skyrmions, given their ability to manifest DMI terms due to their lack of inversion symmetry.[1,3,15,22−24]

In this work we investigate the formation of skyrmionic states via breaking the inversion symmetry of the CrI_3 monolayer by substituting iodine atoms with chloride atoms (Cl_x). Unlike external electric fields, these defects produce localized atomic-scale distortions, which holds the promise of creating fine-tuned distortion patterns and, accordingly, may enable the formation of complex magnetic structures.

METHODOLOGY

Monolayer CrI_3 was represented using the isolated periodic slab model. The initial positions of atoms correspond to the bulk CrI_3 lattice as determined through single-crystal X-ray diffraction at 90 K.[8] To find the optimal structure of the monolayer and its electronic properties, we performed *ab initio* simulations based on density functional theory (DFT) as implemented in the Vienna *ab initio* simulation program (VASP).[25,26] The projector augmented wave method and Perdew−Burk−Ernzerhof exchange correlation functional were used.[27,28] The calculations were performed in the spin-polarized mode. A plane-wave basis set was used with an energy cutoff of 600 eV, and the DFT-D3(0)[29] method was used for dispersion correction. All internal coordinates were fully relaxed. It has been noted that the Hubbard U correction applied within the DFT+U method does not significantly affect the results of the calculations and as such is not used herein.[7,20]

To find the properties of pristine CrI_3, we used a supercell containing two chromium and six iodine atoms. A 3.5 nm vacuum gap in the off-plane direction (z) was used to avoid monolayer interactions with its periodic images. The Brillouin zone was sampled with a Monkhorst−Pack k-point mesh of 6 × 6 × 2. The optimal lattice constant (a_0) was found to be 6.929 Å, which is in close agreement with the experimentally observed value of 6.866 Å.[8]

The calculated Heisenberg isotropic symmetric exchange coefficient (J = −2.99 meV) and the magnetic anisotropy energy (MAE; 0.58 meV/Cr) are comparable with those previously reported for the CrI_3 systems (less than 10 layers): J = −2.2 meV and MAE = 0.65 meV/Cr.[3,7,30]

In order to examine the magnetic effects of Cl substitution, we used a CrI_3 supercell of 1.8 nm × 3.1 nm × 2.0 nm. Several I atoms near a chromium center were replaced with Cl atoms, and the internal coordinates were optimized for each case. The cutoff for energy minimization with respect to the atomic coordinates was set to 10^{-5} eV. With the optimized structure, a noncollinear (NC) spin calculation was run with the self-consistent-field (SCF) convergence cutoff set to 10^{-6} eV. The noncollinear wavefunction was used as a guess for the calculations incorporating spin−orbit coupling effects (NC-SOC) with the SCF convergence set to 10^{-9} eV in order to capture the energy cost of spin rotations, which typically are on the order of 10^{-6}−10^{-4} eV in magnitude.[3]

https://doi.org/10.1021/jacsau.1c00142
JACS Au 2021, 1, 1362−1367

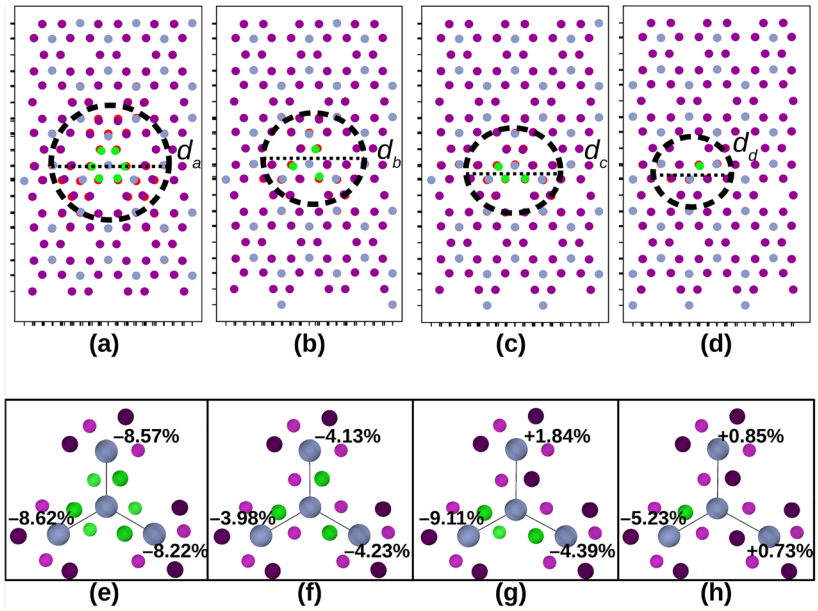

Figure 2. Optimized geometries of the Cl_x:CrI_3 systems. The initial position of the relevant atoms can be visualized by the red circles. The final geometries are shown with the gray circles representing Cr atoms, the purple circles representing iodine atoms, and the green circles representing chlorine atoms after optimization. The geometries consist of Cl_6:CrI_3 (a), Cl_3^a:CrI_3 (b), $Cl_2^aCl^b$:CrI_3 (c), and Cl:CrI_3 (d). (e−h) The four central Cr atoms and bound halogen atoms. The values show the difference in the bond length between the central Cr atom and those neighboring from the pure CrI_3 system and the optimized, doped systems (shown as ±% of the original Cr−Cr bond length).

RESULTS AND DISCUSSION

Geometric Distortion

To investigate the coupling between the lattice distortions in CrI_3 and its magnetic properties, we considered several configurations of Cl substituted for I. Chlorine was specifically chosen, as it has been previously shown that bulk $CrCl_3$ exhibits an in-plane ferromagnetism,[8] which was thought could be taken advantage of to promote skyrmion formation without drastically altering the properties of the CrI_3 layer. Also, of the CrX_3 systems commonly examined, Cl has the smallest atomic radius (i.e., the largest mismatch with that of I) and as such is thought to give rise to the largest geometric distortions. Four Cl_x:CrI_3 structures were examined and can be viewed in the insets for Figure 1. The four configurations considered have six iodine atoms replaced around a chromium center (Cl_6:CrI_3), three Cl atoms replacing the iodine above the chromium atomic plane (Cl_3^a:CrI_3), three Cl atoms replacing two iodine atoms above and one iodine atom below the chromium atomic plane ($Cl_2^aCl^b$:CrI_3), and one Cl atom replacing a single iodine atom (Cl:CrI_3).

As can be seen in Figure 2, replacing I atoms with Cl atoms results in a contraction of the Cr−Cl bonds (in comparison to the Cr−I bonds), as is expected given that Cl is both smaller and more electronegative than I. In the case where six I atoms are replaced, the geometric distortions extend through the monolayer for ∼1.7 nm, similar to the extent of skyrmion formation that has been observed when CrI layers are exposed to a field.[3] It should be noted that this size may be artificially constrained due to the size of the cluster used, as was also noted for the skyrmion formation by Liu et al.[3] This distortion is shown in Figure 2a as a circle of diameter d_a = 1.7 nm. For systems where less Cl has been doped into the cell (in Figure 2b−d) the extent of the distortion caused is lessened. Cl_3^a:CrI_3 shows an extent of d_b = 1.2 nm, and $Cl_2^aCl^b$:CrI_3 and Cl:CrI_3 (d_c and d_d, respectively) show an extent of 1.0 nm.

The effects of the larger spatial extent of the distortion mean that there are additional chromium centers that no longer have the full octahedral symmetry surrounding them. In an octahedral crystal field, Cr(III) d orbitals split into t_{2g} and e_g manifolds. The threefold degenerate t_{2g} levels are singly occupied by three d electrons. This configuration corresponds to a high-spin $^4A_2$ ground state at each Cr site, with the excited $^4T_2$ state being 1.5 eV above. Upon doping Cl in CrI_3, the structure around Cr(III) deviates from the perfect octahedral environment. However, the perturbation is not strong enough to alter the ligand field, and each Cr(III) center still retains the high-spin configuration. The loss of octahedral symmetry gives rise to DMI terms potentially leading to noncollinear spin solutions with no applied field. It is of particular interest that both the Cl_6:CrI_3 and Cl_3^a:CrI_3 systems have a symmetrical distortion around the central Cr and thus the final geometries are similar, while the $Cl_2^aCl^b$:CrI_3 and Cl:CrI_3 systems are less symmetrical about the central Cr. In the case of the $Cl_2^aCl^b$:CrI_3 and Cl:CrI_3 systems the central Cr is pulled slightly toward the Cr centers that are mediated by Cl atoms, leading to a significant distortion of the angles and bond lengths of the surrounding systems.

The formation energy of each isovalent-doped Cl_x:CrI_3 configuration can be estimated by

$$\Delta E = E(Cl_x{:}CrI_3) - E(CrI_3) + n(\mu_I - \mu_{Cl}) \quad (2)$$

where $E(Cl_x{:}CrI_3)$ is the energy of the Cl_x:CrI_3 system, $E(CrI_3)$ is the energy of the CrI_3 lattice without dopants, and n is the number of substituted ions. The chemical potentials, μ, for the iodine and chloride atoms are computed as $(1/2)E(I_2)$ and $(1/2)E(Cl_2)$, respectively. The formation energies given in Table 1 show that the geometries most likely to appear are the singly doped Cl_1:CrI_3 and the symmetrical Cl_6:CrI_3.

As a result of the geometric distortions, the inversion symmetry for the doped systems (except the Cl_6:CrI_3 system) is broken. Thus, the DMI terms become nonzero. The DMI

https://doi.org/10.1021/jacsau.1c00142
JACS Au 2021, 1, 1362−1367

Table 1. Formation Energies, as Determined by Eq 2 for the Four Doped Geometries

system	formation energy (eV)
Cl_6:CrI_3	−3.96
Cl_3^a:CrI_3	28.06
$Cl_2^aCl^b$:CrI_3	27.99
Cl:CrI_3	−0.69

vectors for the Cr atoms within the distorted areas marked in Figure 2 are plotted in Figure 3. This effect is localized to the

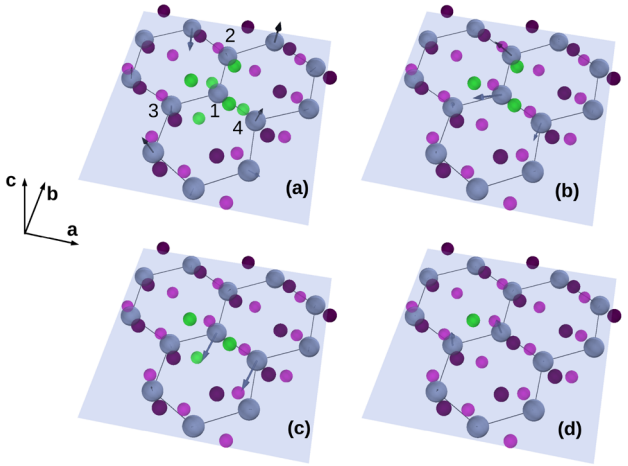

Figure 3. DMI vectors (in black, determined as in ref 31) on each Cr atom from the geometry-optimized, Cl-doped systems shown in Figure 2: (a) Cl_6:CrI_3; (b) Cl_3^a:CrI_3; (c) $Cl_2^aCl^b$:CrI_3; (d) Cl:CrI_3. Since the DMI vectors are only nonzero where the inversion symmetry is broken, and the symmetry breaking is a localized effect, only the atoms that lie roughly within the black circle in Figure 2 have been plotted. The labeled atoms in (a) are the Cr atoms used in the four-state method to calculate the DMI vectors that are reported in Table 2.

areas with geometric distortion. This can be seen in Figure 3d, where the spatial extent of the geometry distortion is significantly less than in the other systems, by the fact that the Cr atoms on the far right (where there was little to no distortion) do not have applicable DMI vectors. As was previously mentioned, the Cl_6:CrI_3 system is able to maintain inversion symmetry around the central atom, and as such the DMI contributions along each halide pathway cancel out, which is not the case for the other systems.

Formation of Spin Bubbles

Magnetic skyrmions are local whirls of the spins that both have a fixed chirality and do a full spin rotation.[1,2,5] Unfortunately, none of the geometries attempted in this study are able to realize a full symmetric skyrmion at zero field. Instead, spin bubbles, localized spin-canted solutions driven by DMI terms, can be observed in the CrI_3 monolayers arising from spin noncollinear solutions. In the case of the Cl:CrI_3 system a spin-bubble solution was stabilized, as can be seen in Figure 4. Plotted in Figure 4 are the atomic clusters shown in Figure 3 with the magnetization vectors for each Cr atom plotted. It can be noted that, in the case of the Cl_3^a:CrI_3 and $Cl_2^aCl^b$:CrI_3 systems, the spin bubble is unable to be manifested and the ferromagnetic solution persists.

In the case of the Cl:CrI_3 system, the stabilization by the formation of the spin bubble over the ferromagnetic solution is

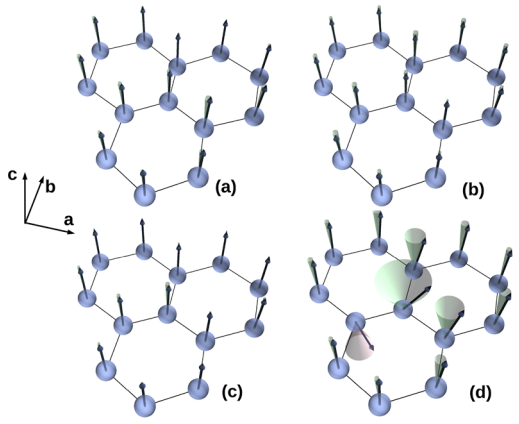

Figure 4. Canted spin states for each of the geometry-optimized, Cl doped systems shown in Figure 2, (a) Cl_6:CrI_3, (b) Cl_3^a:CrI_3, (c) $Cl_2^aCl^b$:CrI_3, and (d) and Cl:CrI_3 resulting from the presence of the doped Cl. Magnetic vectors are shown by black vectors on each Cr atom. The difference between the canted spins and the collinear spins perpendicular to the crystal plane are shown by the cones (where green cones are spins above the layer and red cones are spins beneath the layer).

25.7 meV/Cr. This energetic difference is larger than what has been previously observed, as the stabilization energy from the formation of skyrmions through the use of external fields (∼3 meV/Cr) is much larger than the cost of a spin rotation (<1 meV/Cr).[3] Thus, similarly to the skyrmions formed through the application of external fields, the spin bubbles are topologically protected spin configurations. It is interesting to note that, while it is able to form in the Cl:CrI_3 system, a spin-bubble configuration is not manifested in the $Cl_2^aCl^b$:CrI_3 system. Even though, in the $Cl_2^aCl^b$:CrI_3 system, there is both a lack of symmetry in the geometry (as in either the Cl_6:CrI_3 or Cl_3^a:CrI_3 cases) and there exists a pathway with only a single Cl atom that has a geometric distortion similar to that of the Cl:CrI_3 system. This can be seen in Figure 2g,h, with a 4.39% reduction in Cr−Cr distance for $Cl_2^aCl^b$:CrI_3 in comparison to a 5.23% reduction for Cl:CrI_3. It was previously noted that a minimum field was required in order to induce skyrmions which introduced a distortion between the Cr and I layers in the monolayer CrI_3.[3] Measuring geometric changes for the systems finds that the $Cl_2^aCl^b$:CrI_3 system has a distortion of 2.2% while the Cl:CrI_3 system has a distortion of 3.1%. The distortion of the $Cl_2^aCl^b$:CrI_3 system being less than the previously determined minimum may contribute to why a magnetic bubble state is unable to be manifested even though there are DMI vectors present.

In order to gain insights into the formation of the spin bubble in the Cl:CrI_3 system, the DMI vectors were calculated for the Cr atoms shown in Figure 3. The numerical values for the DMI vectors are given in Table 2 and calculated through the four-state method detailed in refs 15 and 20. This method takes specific chromium pairs (labeled in the table) and directs their local spin orientations in order to extract the energetic values of the coupling between the select centers and their DMI vectors. For the Cl_6:CrI_3 and Cl_3^a:CrI_3 systems only the Cr_1 and Cr_2 pair were calculated due to the presence of the rotational symmetry. For the other systems, the DMI vectors for the nearest neighbors to the central Cr were all explicitly calculated. Previous work has identified that skyrmions are more likely to form when values of $\frac{D_{ij}}{J_{ij}}$ (where $D_{ij} = |\mathbf{D}_{ij}|$) are

https://doi.org/10.1021/jacsau.1c00142
JACS Au 2021, 1, 1362−1367

Table 2. DMI Vectors Calculated Using the Four-State Method of Refs 15 and 20[a]

system	pair	D_{ij}^X (meV)	D_{ij}^Y (meV)	D_{ij}^Z (meV)	J_{ij} (meV)	$\lvert D_{ij}\rvert/J_{ij}$ (meV)
Cl_6:CrI_3	Cr_1−Cr_2	−0.28	0.34	−0.22	−0.07	7.24
Cl_3^a:CrI_3	Cr_1−Cr_2	−0.90	0.79	−1.47	−0.86	2.20
$Cl_2^aCl^b$:CrI_3	Cr_1−Cr_2	0.22	0.72	1.02	−1.38	0.92
$Cl_2^aCl^b$:CrI_3	Cr_1−Cr_3	0.22	1.81	0.21	−1.24	1.48
$Cl_2^aCl^b$:CrI_3	Cr_1−Cr_4	0.26	−0.02	−0.77	−0.08	10.16
Cl:CrI_3	Cr_1−Cr_2	−0.38	−0.16	1.15	−0.89	1.37
Cl:CrI_3	Cr_1−Cr_3	0.22	−0.09	−0.56	−0.68	0.89
Cl:CrI_3	Cr_1−Cr_4	−0.13	−0.52	0.07	−1.16	0.47

[a]For Cl_6:CrI_3 and Cl_3^a:CrI_3, the threefold symmetry surrounding the Cr center is maintained; thus, only one vector is shown. For the other systems, this symmetry is broken and the DMI vectors between the central Cr and the three surrounding Cr centers are shown. Cr centers are identified in Figure 3.

between 0.1 and 0.2 meV.[4,15] Larger values of $\frac{D_{ij}}{J_{ij}}$ favor faster spin rotations about $\mathbf{D}_{ij}$, leading to smaller skyrmions.[4] Our values for $\frac{D_{ij}}{J_{ij}}$ are significantly larger than those reported for previous CrI_3 systems. This is most likely due to the increased localized distortion surrounding the Cr centers. The values for $|\mathbf{D}_{ij}|$ are also larger than those previously reported,[15] though it should be noted that large values for the DMI vectors have been shown in previous studies and will often introduce spin configurations other than skyrmions.[4] Although the Cl:CrI_3 (Cr_1,Cr_3) and $Cl_2^aCl^b$:CrI_3 (Cr_1,Cr_4) systems are close in geometry and as such are expected to both exhibit spin-canted solutions, the $Cl_2^aCl^b$:CrI_3 system has a $\frac{D_{1,4}}{J}$ value (given in Table 2) that is too large to manifest a stable spin whirl solution at zero field. In contrast, while the value for $\frac{D_{ij}}{J}$ is larger than in other reports of skyrmion-forming monolayer chromium iodide systems, a spin canted solution is still able to manifest for the Cl:CrI_3 system.

CONCLUSION

We show that, upon substituting select I atoms in a CrI_3 monolayer with Cl atoms, localized spin-bubble states form. These spin states arise from the lattice distortions induced by the ionic radii mismatch between the host and the defect species. While distortions are driven by the difference in the X−Cr bond lengths, the interactions between these distortions can induce long-range directional lattice polarization that may enable coupling between spatially separated spin-bubble states. It was noted that, when these spin-bubble systems formed, they were topologically protected. They were significantly more stable than either the cost of a spin flip or the stabilization noted by electric-field-induced skyrmions. This work provides an important step toward manifesting skyrmions under conditions that would be useful for spintronic applications by potentially reducing the field required and increasing the operating temperature through controlled doping of CrI_3 monolayers.

AUTHOR INFORMATION

Corresponding Author

Xiaosong Li − *Department of Chemistry, University of Washington, Seattle, Washington 98195, United States; Pacific Northwest National Laboratory, Richland, Washington 99354, United States;* orcid.org/0000-0001-7341-6240; Email: xsli@uw.edu

Authors

Ryan A. Beck − *Department of Chemistry, University of Washington, Seattle, Washington 98195, United States;* orcid.org/0000-0002-2953-970X

Lixin Lu − *Department of Chemistry, University of Washington, Seattle, Washington 98195, United States;* orcid.org/0000-0003-3203-4822

Peter V. Sushko − *Physical Sciences Division, Physical & Computational Sciences Directorate, Pacific Northwest National Laboratory, Richland, Washington 99352, United States;* orcid.org/0000-0001-7338-4146

Xiaodong Xu − *Department of Physics, University of Washington, Seattle, Washington 98195, United States;* orcid.org/0000-0003-0348-2095

Complete contact information is available at: https://pubs.acs.org/10.1021/jacsau.1c00142

Notes

The authors declare no competing financial interest.

ACKNOWLEDGMENTS

The study of two-dimensional magnetic materials was supported by the Northwest Institute for Materials Physics, Chemistry, and Technology (NW-IMPACT) and the University of Washington Molecular Engineering Materials Center (DMR-1719797). P.V.S. was supported by the Chemical Dynamics Initiative funded via PNNL's LDRD Program. X.L. acknowledges support from the National Science Foundation (CHE-1856210) for developing theories to investigate magnetic properties. This work was facilitated though the use of advanced computational, storage, and networking infrastructure provided by the Hyak supercomputer system and funded by the STF at the University of Washington.

REFERENCES

(1) Fert, A.; Reyren, N.; Cros, V. Magnetic Skyrmions: Advances in Physics and Potential Applications. *Nat. Rev.* **2017**, *2*, 17031.

(2) Bogatyrëv, A. B.; Metlov, K. L. What Makes Magnetic Skyrmions Different from Magnetic Bubbles? *J. Magn. Magn. Mater.* **2018**, *465*, 743−746.

(3) Liu, J.; Shi, M.; Mo, P.; Lu, J. Electrical-Field-Induced Magnetic Skyrmion Ground State in a Two-Dimensional Chromium Tri-Iodide Ferromagnetic Monolayer. *AIP Adv.* **2018**, *8*, 055316.

(4) Fert, A.; Cros, V.; Sampaio, J. Skyrmions on the Track. *Nat. Nanotechnol.* **2013**, *8*, 152−156.

(5) Ding, B.; Li, Z.; Xu, G.; Li, H.; Hou, Z.; Liu, E.; Xi, X.; Xu, F.; Yao, Y.; Wang, W. Observation of Magnetic Skyrmion Bubbles in a van der Waals Ferromagnet Fe_3GeTe_2. *Nano Lett.* **2020**, *20*, 868−873.

(6) Moriya, T. Anisotropic Superexchange Interaction and Weak Ferromagnetism. *Phys. Rev.* **1960**, *120*, 91−98.
(7) Lado, J. L.; Fernández-Rossier, J. On the Origin of Magnetic Anisotropy in Two Dimensional CrI_3. *2D Mater.* **2017**, *4*, 035002.
(8) McGuire, M. A.; Dixit, H.; Cooper, V. R.; Sales, B. C. Coupling of Crystal Structure and Magnetism in the Layered Ferromagnetic Insulator CrI_3. *Chem. Mater.* **2015**, *27*, 612−620.
(9) McGuire, M. A. Crystal and Magnetic Structures in Layered, Transition Metal Dihalides and Trihalides. *Crystals* **2017**, *7*, 121.
(10) Huang, B.; Clark, G.; Navarro-Moratalla, E.; Klien, D. R.; Cheng, R.; Seyler, K. L.; Zhong, D.; Schmidgall, E.; McGuire, M. A.; Cobden, D. H.; Yao, W.; Xiao, D.; Jarillo-Herrero, P.; Xu, X. Layer-Dependent Ferromagnetism in a van der Waals Crystal Down to the Monolayer Limit. *Nature* **2017**, *546*, 270−273.
(11) Huang, B.; Clark, G.; Klein, D. R.; MacNeill, D.; Navarro-Moratalla, E.; Seyler, K. L.; Wilson, N.; McGuire, M. A.; Cobden, D. H.; Xiao, D.; Yao, W.; Jarillo-Herrero, P.; Xu, X. Electrical Control of 2D Magnetism in Bilayer CrI_3. *Nat. Nanotechnol.* **2018**, *13*, 544−548.
(12) Song, T.; et al. Switching 2D Magnetic States via Pressure Tuning of layer Stacking. *Nat. Mater.* **2019**, *18*, 1476−4660.
(13) Sivadas, N.; Okamoto, S.; Xu, X.; Fennie, C. J.; Xiao, D. Stacking-Dependent Magnetism in Bilayer CrI_3. *Nano Lett.* **2018**, *18*, 7658−7664.
(14) Lee, C.; Kwon, H. Y.; Kim, N. J.; Yoon, H. G.; Song, C.; Lee, D. B.; Choi, J. W.; Son, Y.-W.; Won, C. Magnetic Structures in the Locally Inverted Interlayer Coupling Region of a Bilayer Magnetic System. *J. Magn. Magn. Mater.* **2020**, *501*, 166447.
(15) Xu, C.; Feng, J.; Prokhorenko, S.; Nahas, Y.; Xiang, H.; Bellaiche, L. Topological Spin Texture in Janus Monolayers of the Chromium trihalides $Cr(I,X)_3$. *Phys. Rev. B: Condens. Matter Mater. Phys.* **2020**, *101*, 060404.
(16) Felser, C.; Fecher, G. H.; Balke, B. Spintronics: A Challenge for Materials Science and Solid-State Chemistry. *Angew. Chem., Int. Ed.* **2007**, *46*, 668−699.
(17) Behin-Aein, B.; Wang, J.-P.; Wiesendanger, R. Computing with Spins and Magnets. *MRS Bull.* **2014**, *39*, 696−702.
(18) Handy, L. L.; Gregory, N. W. A Study of the Chromous-Chromic Iodide Equilibrium. *J. Am. Chem. Soc.* **1950**, *72*, 5049−5051.
(19) Mermin, N. D.; Wagner, H. Absence of Ferromagnetism or Antiferromagnetism in One- or Two- Dimensional Isotropic Heisenberg Models. *Phys. Rev. Lett.* **1966**, *17*, 1133.
(20) Xu, C.; Feng, J.; Xiang, H.; Bellaiche, L. Interplay Between Kitaev Interaction and Single Ion Anisotropy in Ferromagnetic CrI_3 and $CrGeTe_3$ Monolayers. *Comp. Mater.* **2018**, *4*, 57.
(21) Anderson, P. W. Antiferromagnetism, Theory of Superexchange Interaction. *Phys. Rev.* **1950**, *79*, 350−356.
(22) Liu, J.; Shi, M.; Lu, J.; Anantram, M. P. Analysis of Electrical-Filed-Dependent Dzyaloshinskii-Moriya Interaction and Magneto-crystalline Anisotropy in a Two-Dimensional Ferromagnetic Monolayer. *Phys. Rev. B: Condens. Matter Mater. Phys.* **2018**, *97*, 054416.
(23) Behera, A. K.; Chowdhury, S.; Das, S. R. Magnetic Skyrmions in Atomic This CrI_3 Monolayer. *Appl. Phys. Lett.* **2019**, *114*, 232402.
(24) Albaridy, R.; Manchon, A.; Schwingenschlögl, U. Tunable Magnetic Anisotropy in Cr-Trihalide Janus Monolayers. *J. Phys.: Condens. Matter* **2020**, *32*, 355702.
(25) Kresse, G.; Furthmüller, J. Efficiency of Ab-Initio Total Energy Calculations for Metals and Semiconductors Using a Plane-Wave Basis Set. *Comput. Mater. Sci.* **1996**, *6*, 15−50.
(26) Kresse, G.; Furthmüller, J. Efficient Iterative Schemes for ab initio Total-Energy Calculations Using a Plane-Wave Basis Set. *Phys. Rev. B: Condens. Matter Mater. Phys.* **1996**, *54*, 11169.
(27) Blöchl, P. E. Projector Augmented-Wave Method. *Phys. Rev. B: Condens. Matter Mater. Phys.* **1994**, *50*, 17953.
(28) Perdew, J. P.; Burke, K.; Ernzerhof, M. Generalized Gradient Approximation Made Simple. *Phys. Rev. Lett.* **1996**, *77*, 3865−3868.
(29) Grimme, S.; Antony, J.; Ehrlich, S.; Krieg, S. A Consistent and Accurate ab initio Parametrization of Density Functional Dispersion Correction (DFT-D) for the 94 elements H-Pu. *J. Chem. Phys.* **2010**, *132*, 154104.
(30) Wang, C.; Gao, Y.; Lv, H.; Xu, X.; Xiao, D. Stacking Domain Wall Magnons in Twisted van der Waals Magnets. *Phys. Rev. Lett.* **2020**, *125*, 247201.
(31) Keffer, F. Moriya Interaction and the Problem of the Spin Arrangements in βMnS. *Phys. Rev.* **1962**, *126*, 896−900.

https://doi.org/10.1021/jacsau.1c00142
JACS Au 2021, 1, 1362−1367